

The Gamow-state description of the decay energy spectrum of neutron-unbound ^{25}O

R.M. Id Betan,^{1,2,3} R. de la Madrid⁴

¹*Physics Institute of Rosario (CONICET), Esmeralda y Ocampo, S2000EZP Rosario, Argentina.*

²*Department of Physics FCEIA (UNR), Av. Pellegrini 250, S2000BTP Rosario, Argentina.*

³*Institute of Nuclear Studies and Ionizing Radiations (UNR), Riobamba y Berutti, S2000EKA Rosario, Argentina.*

⁴*Department of Physics, Lamar University, Beaumont, TX 77710, United States.*

Abstract

We show the feasibility of calculating the decay energy spectrum of neutron emitting nuclei within the Gamow-state description of resonances by obtaining the decay energy spectrum of ^{25}O . We model this nucleus as a valence neutron interacting with an ^{24}O inert core, and we obtain the resulting resonant energies, widths and decay energy spectra for the ground and first excited states. We also discuss the similarities and differences between the decay energy spectrum of a Gamow state and the Breit-Wigner distribution with energy-dependent width.

Key words: Exact solutions, Single-particle levels, Nuclear structure models, ^{25}O strength function

PACS: 04.20.Jb, 21.10.Pc, 21.60.-n, 27.80.+w

1 Introduction

Ever since the discovery of the exotic ^{11}Li nucleus [1], there have been many experimental [2–4] and theoretical [5–7] studies of nuclei far from the beta stability line. On the experimental side, new techniques were developed to produce and study the properties of rare isotopes. On the theoretical side, new models were developed to guide and explain the experimental findings. The theoretical and experimental understanding of unstable nuclei will continue to be one of the main goals of the nuclear physics community [8], as testified by the construction and updating of a number of facilities around the world [9–12].

Experimentally, one method of studying unstable nuclei is by means of their decay energy spectrum, which measures the number of decays per unit of energy versus energy (see for example Refs. [13,14]). In particular, by using techniques such as invariant-mass spectroscopy, it is possible to obtain the experimental decay energy spectrum of some unstable nuclei that decay by neutron emission (see for example Refs. [3,15–17]). Hence, it is important to be able to calculate such spectra theoretically.

In Refs. [18,19], the resonant (Gamow) state was used to obtain a theoretical expression for the decay energy spectrum of an unstable system decaying into the continuum. The purpose of the present paper is to use the formalism of Refs. [18,19] to obtain the energy spectrum of the ^{25}O nucleus, which decays by neutron emission.

Dripline Oxygen isotopes are currently of great interest, both theoretically and experimentally. From the excited states of ^{19}O [20] to the isotopes well beyond the neutron drip line [21], there are several Oxygen isotopes whose energies, widths, and decay energy spectra can be used as a test bench for different theories. The heavier neutron drip line nucleus that has been observed experimentally is ^{24}O , which was found to be doubly magic [22]. An excited state of ^{24}O was found [23] to decay sequentially to ^{22}O . In addition, other low-lying neutron-unbound excited states of ^{24}O have been measured [24]. The energy and width of the unbound ground state of ^{25}O were investigated in Refs. [25–28], and strong evidence for the first excited state of ^{25}O was found in Ref. [28]. The ground state [27,29], excited states and decay modes [17,26] of ^{26}O have also been studied.

In our analysis, we will use the neutron-unbound ^{25}O because its decay energy spectrum has been measured experimentally [25–28]. Since ^{24}O is doubly magic, we will treat ^{25}O as a valence neutron in an ^{24}O core, and we will describe the valence neutron by a Gamow state. This two-body model is able to reproduce the experimental ground state of ^{25}O , $3/2^+$. However, our two-body model yields $7/2^-$ as the first excited state, instead of the one found experimentally, $1/2^+$.

The structure of the paper is as follows. In Sec. 2, we summarize the formalism needed to calculate the theoretical decay energy spectrum. In Sec. 3, we assess the validity of the code. In Sec. 4, we apply the code to the ^{25}O nucleus. We will model the interaction between the valence neutron and the ^{24}O core by the Woods-Saxon and the spin-orbit potentials, and obtain the energies, widths and decay energy spectra of the ground and first excited states. We will compare our results with those obtained by the Continuum and the Gamow Shell Models [6,7]. We will also compare the theoretical decay energy spectrum with the experimental ones [25–28]. In addition, we will discuss the similarities and differences (both quantitative and phenomenological) between the

Gamow-state decay energy spectra and the Breit-Wigner distributions with energy-dependent width. In Sec. 5, we summarize our main results and present an outlook of future applications.

2 Formalism

In order to be self-contained, in this section we outline the main ingredients needed to calculate the decay energy spectrum of ^{25}O .

2.1 The decay energy spectrum of a Gamow state

Let $H = H_0 + V$ be the Hamiltonian that describes the decaying system, formed in our model by an inert ^{24}O core and a valence neutron. The free Hamiltonian H_0 is the part of the Hamiltonian that describes the valence neutron after it has been ejected and is far away from the core, whereas V is the interaction potential between the core and the valence neutron. Let us describe the unstable state by a Gamow [31] state $|z_{\text{R}}\rangle$ such that $H|z_{\text{R}}\rangle = z_{\text{R}}|z_{\text{R}}\rangle$ and $z_{\text{R}} = E_{\text{R}} - i\Gamma_{\text{R}}/2$. Then, the differential decay width $\frac{d\bar{\Gamma}}{dE}$, which describes the strength of the interaction between the resonance and the continuum at each scattering energy E , is given by [18]

$$\frac{d\bar{\Gamma}(E)}{dE} = 2\pi L(E) |\langle E|V|z_{\text{R}}\rangle|^2, \quad (1)$$

where $L(E)$ is the Lorentzian distribution

$$L(E) = \frac{1}{\pi} \frac{\Gamma_{\text{R}}/2}{(E - E_{\text{R}})^2 + (\Gamma_{\text{R}}/2)^2}, \quad (2)$$

and $|E\rangle$ is an eigenstate of the free Hamiltonian with energy E , $H_0|E\rangle = E|E\rangle$.

The normalized, theoretical decay energy spectrum of a resonance decaying into the continuum is then obtained as [18]

$$\frac{dP(E)}{dE} = \frac{1}{\bar{\Gamma}} \frac{d\bar{\Gamma}(E)}{dE} = \frac{2\pi}{\bar{\Gamma}} L(E) |\langle E|V|z_{\text{R}}\rangle|^2, \quad (3)$$

where $\bar{\Gamma}$ is the total decay width,

$$\bar{\Gamma} = \int_0^\infty \left(\frac{d\bar{\Gamma}}{dE} \right) dE = 2\pi \int_0^\infty L(E) |\langle E|V|z_{\text{R}}\rangle|^2 dE. \quad (4)$$

We will identify the theoretical spectrum of Eq. (3) with the experimental decay energy spectrum.

It should be noted that $\bar{\Gamma}$ is in general different from Γ_{R} , and therefore $\bar{\Gamma}$ is not related to the lifetime of the resonance. Physically, we can interpret $\bar{\Gamma}$ as a measure of the overall strength of the interaction between the resonance and the continuum. This is why in Sec. 4 we will use $\bar{\Gamma}$ to quantify the relative strength of the spectra of different resonances.

It should also be noted that Eqs. (3) and (4) represent, in a way, an extension of Fermi's Golden Rule to the case where the broadening of the decay energy spectrum is taken into account. Such broadening is provided by the Breit-Wigner distribution.

2.2 The Schrödinger equation of the valence neutron

Because ^{24}O is a doubly magic nucleus [22], we are going to neglect the many-body nature of ^{25}O and treat it as an ^{24}O core plus a single neutron that is subject to a mean-field potential created by the ^{24}O core. As it is customary, we will model such mean-field potential by the Woods-Saxon potential and a spin-orbit interaction,

$$V(r) = V_{\text{ws}}(r) + V_{\text{so}}(r) = -V_0 f(r) + V_{\text{so}} \frac{1}{r} \frac{df(r)}{dr} \xi_{l,j}, \quad (5)$$

where $V_0 > 0$ represents the potential well depth, and $V_{\text{so}} > 0$ represents the strength of the spin-orbit interaction. The function $f(r)$ is given by

$$f(r) = \frac{1}{1 + \exp\left(\frac{r-R}{a}\right)}, \quad (6)$$

where a is the diffuseness parameter (or surface thickness), and $R = r_0 A^{1/3}$ is the nuclear radius, A being the mass number. The function $\xi_{l,j}$ is given by

$$\xi_{l,j} = \begin{cases} \frac{l}{2} & \text{for } j = l + \frac{1}{2}, \\ -\frac{(l+1)}{2} & \text{for } j = l - \frac{1}{2}, \end{cases} \quad (7)$$

where l and j are the orbital and the total angular momentum of the valence neutron, respectively.

Due to the spherical symmetry of the potential, we can work with spherical coordinates, separate the radial and angular dependences, and obtain the radial Schrödinger equation for each partial wave,

$$\left(\frac{-\hbar^2}{2\mu} \frac{d^2}{dr^2} + \frac{\hbar^2 l(l+1)}{2\mu r^2} + V(r) \right) u_l(r; E) = E u_l(r; E), \quad (8)$$

where μ is the reduced mass of the system. By solving Eq. (8) subject to purely outgoing boundary conditions, we obtain the resonant (Gamow) eigenfunctions $u_l(r; z_R)$. When z_R is real and negative, $u_l(r; z_R)$ becomes a bound state. Under the appropriate boundary conditions, Eq. (8) yields the scattering eigenfunctions when E is positive.

After the neutron is expelled from the nucleus, it behaves like a free particle, and therefore its radial wave function $\chi_l(r; E)$ satisfies the radial, free Schrödinger equation,

$$\left(\frac{-\hbar^2}{2\mu} \frac{d^2}{dr^2} + \frac{\hbar^2 l(l+1)}{2\mu r^2} \right) \chi_l(r; E) = E \chi_l(r; E), \quad (9)$$

subject to the boundary condition that the eigenfunction is regular at the origin, $\chi_l(0; E) = 0$. The delta-normalized solution of Eq. (9) that is regular at the origin is given by the reduced Riccati-Bessel function \hat{j}_l (see for example Ref. [32]),

$$\chi_l(r; E) = \sqrt{\frac{2\mu}{\hbar^2}} \frac{1}{\sqrt{k\pi}} \hat{j}_l(kr), \quad (10)$$

where $k = \sqrt{\frac{2\mu}{\hbar^2} E}$ is the wave number. The Riccati-Bessel function can be written [32] in terms of the spherical Bessel function $j_l(z)$ and the ordinary Bessel function $J_\lambda(z)$ as $\hat{j}_l(z) = z j_l(z) = \sqrt{\frac{\pi z}{2}} J_{l+1/2}(z)$.

By combining Eq. (3) with the Gamow eigenfunction $u_l(r; z_R)$ and with the free, radial eigenfunction $\chi_l(r; E)$, we can obtain the theoretical decay energy spectrum of ^{25}O .

3 Validation of the numerical procedure

We have used the code GAMOW [33] to solve numerically the Schrödinger equation (8) in order to obtain the resonant energies and the Gamow states. We have used the code ANTI [34, 35] to obtain the scattering states. The resulting energies and eigenfunctions were afterward plugged into Eq. (3) to obtain the numerical decay energy spectrum. Because the Gamow eigenfunctions diverge exponentially, and because the resonant energies are usually very sensitive to small changes in the parameters of the potential, we performed three tests to validate our numerical procedure.

3.1 First test: The energy density of the free eigenfunctions

In the first test, we calculated the energy density of the free scattering eigenfunctions, $\int dr |\chi_l(r; E)|^2$, using the code ANTI [34,35] and Mathematica [36]. We have plotted the results for $l = 6$ in Fig. 1, where we can see that the plots are essentially the same. In particular, ANTI and Mathematica yield a maximum of 0.7254 MeV^{-1} at the energies of 1.677 MeV and 1.65 MeV, respectively.

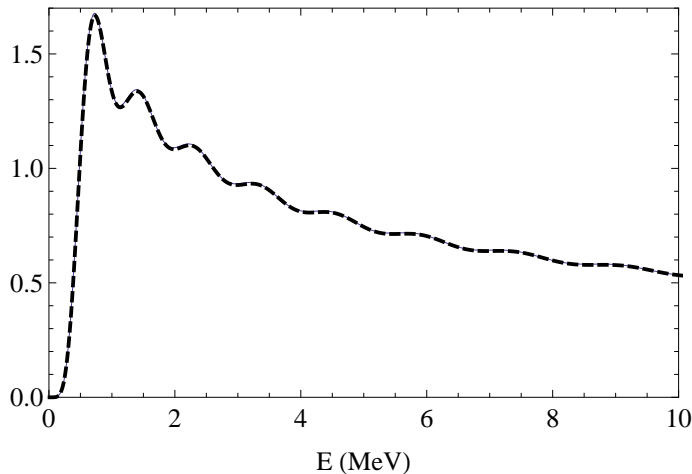


Fig. 1. (Color online) Comparison of the integral $\int_0^{50} |\chi_l(r; E)|^2 dr$ for $l = 6$ and $\frac{2\mu}{\hbar^2} = 0.047892 \text{ MeV}^{-1}\text{-fm}^{-2}$ obtained numerically using Mathematica (thin, blue line) and the code ANTI (thick, dashed, black line). The plots are essentially indistinguishable.

3.2 Second test: Location of the resonant energy in the energy density of the scattering eigenfunctions

In order to test the accuracy of the resonant energies, we compared the real part of such energies with the peaks in the energy density of the scattering eigenfunctions. In this second test, we fixed the parameters of the Woods-Saxon potential so that we can reproduce the lowest energy levels of ^{133}Sn . For simplicity, in this second test we neglected the spin-orbit interaction. The values of the parameters we used are $V_0 = 43.5 \text{ MeV}$ and $R = 6.466 \text{ fm}$ ($r_0 = 1.27 \text{ fm}$). For $l = 6$, we obtained a sharp resonance of complex energy $z_R = (4.460 - i0.014) \text{ MeV}$. We then obtained the scattering eigenfunctions $u_l(r; E)$ of Eq. (8) for $l = 6$. The resulting energy density, $\int |u_l(r; E)|^2 dr$, where r is in fm and $E > 0$ is in MeV, is plotted in Fig. 2.

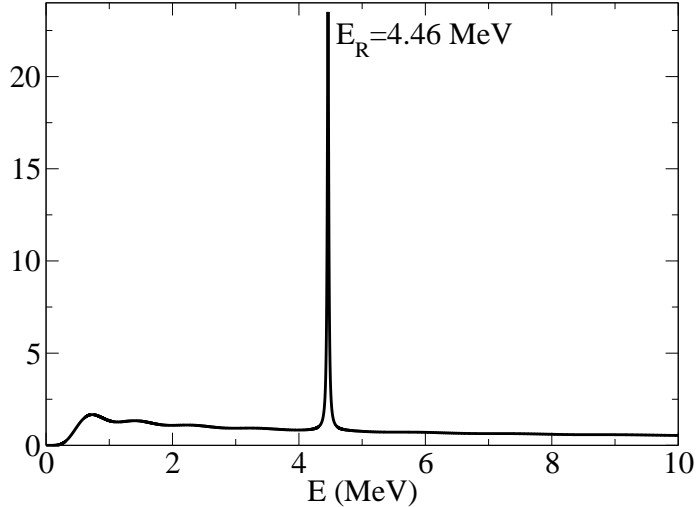


Fig. 2. Plot of the energy density of the scattering eigenfunction, $\int_0^{50} |u_l(r; E)|^2 dr$.

It is clear from Fig. 2 that the radial probability density of the scattering wave function is sharply peaked around the energy 4.46 MeV. This energy coincides with the real part of the resonant energy $z_R = (4.460 - i 0.014)$ MeV.

3.3 Third test: The delta-shell potential

The formalism of Ref. [18] was applied in Ref. [19] to the delta-shell potential $V_\delta(r) = g \delta(r - R)$ for $l = 0$. It was found in Ref. [19] that the s -wave resonant energies of the delta-shell potential can be expressed in terms of the Lambert W function, and therefore one can calculate the resonant energies, decay widths and decay energy spectra of $V_\delta(r)$ exactly. As a third validation of our numerical procedure, we have applied it to an almost delta-shell potential¹ and compared the results with those of Ref. [19].

Our almost delta-shell potential is given by

$$V_a(r) = -g \frac{df(r)}{dr} = \frac{g}{a} \frac{e^{\frac{r-R}{a}}}{\left[1 + e^{\frac{r-R}{a}}\right]^2}, \quad (11)$$

where a is very small. It should be noted that the choice $g > 0$ ($g < 0$) makes the potential repulsive (attractive). As explained in Appendix A, when a is very small, $V_a(r)$ becomes, for practical purposes, the delta-shell potential centered at $r = R$.

Since the potential $V_a(r)$ becomes very singular when a is small, care must be

¹ In Appendix A, we explain in what sense the potential of Eq. (11) is almost a delta-shell potential.

taken in obtaining the resonant energies when a tends to zero. In our case, we used a two-step process to obtain the resonant energies. In the first step, we obtained the resonant energies for decreasing values of a ; in the second step, we extrapolated [37] the result to $a \rightarrow 0$. In this way, we first calculated the $l = 0$ ground (bound) and first excited (unbound) states for the case that $R = 6.466$ fm and $\frac{2\mu}{\hbar^2} = 0.047892$ MeV⁻¹-fm⁻² (which correspond to ¹³³Sn), and for decreasing values of a up to $a = 0.04$ fm. Afterward, we extrapolated the results using four order algebraic extrapolation [37] up to $a = 10^{-5}$ fm.

In order to compare our results with those of Ref. [19], we need to recall that the results of Ref. [19] were given in terms of the dimensionless coupling constant $\lambda = \frac{2\mu}{\hbar^2} Rg$. Hence, with our choice of R and μ ($R = 6.466$ fm and $\frac{2\mu}{\hbar^2} = 0.047892$ MeV⁻¹-fm⁻²), the strength g can be written in terms of λ as $g = 3.229 \lambda$ MeV-fm, and the energies and widths of Ref. [19] are given in units of $\hbar^2/2\mu R^2 = 0.4994$ MeV.

In Table 1, we compare the calculated ground state and first-excited state energies with those of Ref. [19] for $\lambda = -0.5$, -10 , and -100 . As can be seen in Table 1, our numerical results are in fairly good agreement with the exact ones.

Table 1

Comparison of the calculated ground state energy E_{gs} and first excited state energy z_{R} with those of Ref. [19].

Strength		E_{gs} (MeV)		z_{R} (MeV)	
λ	g (MeV)	Exact	Present work	Exact	Present work
-0.5	-1.6146	-0.19711	-0.20554	5.935 - i 5.180	5.895 - i 5.204
-10	-32.29	-12.484	-12.475	5.897 - i 0.356	5.823 - i 0.335
-100	-322.9	-1248.5	-1139.0	5.029 - i 0.00320	5.030 - i 0.00298

The calculation of the decay width of Eq. (4) involves the resonant states and the free scattering states, and therefore constitutes a more demanding test. In Table 2, we compare the calculated decay width with the exact one for the first excited state when $\lambda = -0.5$, -10 , and -100 .

As can be seen in Table 2, our calculated decay width agrees well with the exact one for strong couplings ($\lambda = -10$, -100) but not for weak couplings ($\lambda = -0.5$). The reason why our calculated $\bar{\Gamma}$ is not accurate when λ is small is that, for weak couplings, the resonance is broad, its decay energy spectrum is also broad, and hence its tails are not negligible at energies much higher than the resonant energy. Since our numerical procedure to calculate $\bar{\Gamma}$ omits

Table 2

Comparison of the calculated $\bar{\Gamma}$ with that of Ref. [19] for the first excited state.

Strength		$\bar{\Gamma}$ (MeV)	
λ	g (MeV)	Exact	Present work
-0.5	-1.6146	0.22769	0.0688
-10	-32.29	0.9335	0.825
-100	-322.9	0.01283	0.0127

the high-energy tails, our decay constant is much smaller than the exact one when the coupling is weak.

Overall, our numerical results are accurate for sharp resonances, but not for broad ones. However, since the resonances of ^{25}O are sharp, we expect that our numerical results for ^{25}O to be fairly accurate, except for underestimating the decay widths $\bar{\Gamma}$ due to the neglect of the high-energy tails of the decay energy spectrum.

4 The decay energy spectrum of ^{25}O

In this section, we are going to calculate the decay energy spectrum of the ground state and of the first excited state of the unbound oxygen isotope ^{25}O using a simple two-body model, i.e., one valence neutron outside the ^{24}O core that creates the potential of Eq. (5).

We choose the radius and diffuseness of the mean field potential (the same for the Woods-Saxon and the spin-orbit parts) as in Ref. [38], $a = 0.65$ fm and $r_0 = 1.06$ fm. The Woods-Saxon V_0 and spin-orbit V_{so} strengths are chosen to approximately account for the average 768.5 keV of the experimental ground state energies of ^{25}O reported in Refs. [25] (770 keV), [26] (725 keV), [27] (749 keV) and [28] (830 keV), and for the experimental gap between the ground state energy of ^{25}O with that of the first hole state in the ^{24}O core, $E_{0d_{3/2}} - E_{1s_{1/2}} = 4.857$ MeV [25]. Such criteria, and the experimental neutron separation energy $S_n(^{25}\text{O}) = -0.776$ MeV [39], lead to the following parameters: $V_0 = 57.7$ MeV, and $V_{\text{so}} = 15.32$ MeV-fm².

For the above parameters, the complex energy of the ground state was found to be $z_{d_{3/2}} = (0.766 - i0.034)$ MeV. Thus, the ground state's pole width is $\Gamma_{\text{R},d_{3/2}} = 68$ keV. This pole width is similar to the pole width of the Continuum Shell Model [6] (63 keV), and slightly higher than that of the Gamow Shell Model (the average of the two models used in Ref. [21] yields 49.5 keV, whereas Ref. [28] reports a pole width of 51 keV).

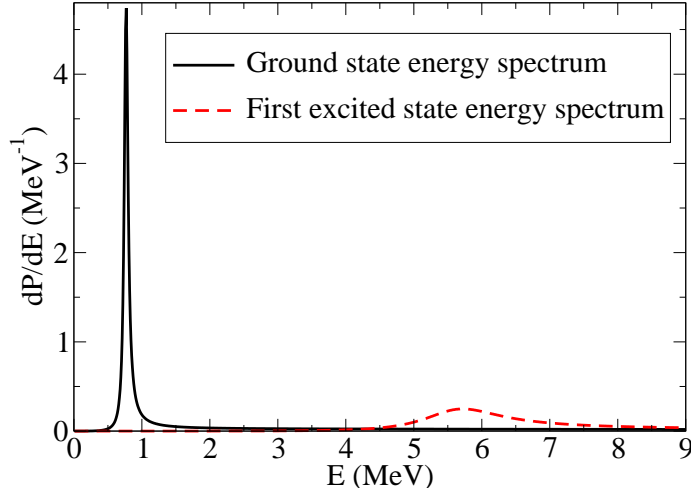


Fig. 3. (Color online) Decay energy spectrum of the ground state $3/2^+$ (solid, black line) and the first excited state $7/2^-$ (red, dashed line) of ^{25}O .

Comparison of $\Gamma_{R,d_{3/2}}$ with the experimental pole widths is not so straightforward, because the experimental pole widths vary wildly (172 keV in Ref. [25], 20 keV in Ref. [26], and 88 keV in Ref. [27]). Their average, 93 keV, is larger than any theoretical pole widths. In fact, the experimental pole widths are usually overestimated, because the experimental error is convoluted with the ideal decay energy spectrum, which makes the experimental decay energy spectrum broader than the ideal one.

In the four-body model of Ref. [28], the first excited state of ^{25}O was reported to be a $1/2^+$ state, and strong experimental evidence for such state was also found [28]. However, our simple two-body model is unable to produce such $1/2^+$ as the first excited state.² Instead, the first excited state of our two-body model is $f_{7/2} = 7/2^-$, whose complex energy is $z_{f_{7/2}} = (5.588 - i0.697)$ MeV. The four-body model of Ref. [28] also produces an $f_{7/2} = 7/2^-$ state, whose complex energy is $5.536 - i0.0075$ MeV. Thus, the energy predicted by our two-body model for the $f_{7/2} = 7/2^-$ state is consistent with that of the four-body model of Ref. [28],³ although our pole width is much larger than that of Ref. [28].

Figure 3 shows the decay energy spectrum of Eq. (3) for the ground state $d_{3/2} = 3/2^+$ and for the first excited state $f_{7/2} = 7/2^-$ of our two-body model. The spectrum of the ground state is a narrow, sharp peak, whereas that of the first excited state is less pronounced and much wider.

² The $1/2^+$ state may be seen as an excitation of the ^{24}O core [40], which in our model is inert.

³ The energy of the $f_{7/2} = 7/2^-$ state reported in Ref. [28] is 4.77 MeV, and it is given with respect to the ground state. Thus, in order to make a proper comparison with the results of Ref. [28], we have added to 4.77 MeV the energy of the ground state $d_{3/2} = 3/2^+$, resulting in $4.77 \text{ MeV} + 0.766 \text{ MeV} = 5.536 \text{ MeV}$.

In Ref. [18], it was proposed that the decay widths can account for the overall strength of the interaction between the resonance and the continuum. In our case, $\bar{\Gamma}_{d_{3/2}} = 0.133$ MeV, and $\bar{\Gamma}_{f_{7/2}} = 2.424$ MeV. Clearly, the coupling with the continuum is much stronger for the first excited state, which makes it less sharp (i.e., less “bound”) than the ground state. It was also proposed in Ref. [18] that one could use the dimensionless decay constant $\Gamma = \frac{\bar{\Gamma}}{\Gamma_R}$ as a measure of the coupling between the resonance and the continuum: The larger Γ , the more “bound” the resonance is, and hence the weaker the coupling to the continuum is. In our case, $\Gamma_{d_{3/2}} = 7.824$, and $\Gamma_{f_{7/2}} = 6.956$. Thus, their dimensionless decay constants also indicate that the ground state is more “bound” than the first excited state, as it should be.

The experimental decay energy spectrum of Ref. [28] was consistent with the inclusion of a first-excited $1/2^+$ state of ^{25}O . The relative cross section of the ground and first excited states was determined to be $\frac{\sigma_{3/2^+}}{\sigma_{1/2^+}} = 4$, which can be interpreted by saying that producing the ground state is four times as likely as producing the first excited state. Using the Gamow-state description of resonances, it is possible to introduce a different way to quantify the relative likelihood of production of two resonances. Since the decay width $\bar{\Gamma}$ quantifies the overall strength of the coupling between the resonance and the continuum, and since resonances with small decay widths would be sharper than those with larger decay widths, we can use the ratio of the decay widths of two resonances as a measure of the relative strength of their decay energy spectra, i.e., as a measure of how likely one can observe the decay energy spectra of a given resonance compared to that of another one. In our model, $d_{3/2} = 3/2^+$ is the ground state and $f_{7/2} = 7/2^-$ is the first excited state, and we have that $\frac{\bar{\Gamma}_{f_{7/2}}}{\bar{\Gamma}_{d_{3/2}}} \sim 18$. This means that, according to our two-body model, it is much more likely to produce the ground state $d_{3/2} = 3/2^+$ than the first-excited state $f_{7/2} = 7/2^-$, as is already clear by visually inspecting their spectra in Fig. 3.

Theoretically, the width of the peaks of decay energy spectra are determined by the pole widths Γ_R rather than by the decay widths $\bar{\Gamma}$, as can be seen in Fig. 3. However, the theoretical pole widths are usually much smaller than the widths of the experimental decay energy spectra. The reason is that the experimental resolution of the detector is usually convoluted with the true decay energy spectrum, and such convolution tends to broaden the spectrum. Thus, in order to compare our theoretical formula with experiment, we would need to deconvolute the experimental resolution from the true decay energy spectrum.

The resonant peaks in experimental decay energy spectra are usually fitted with symmetric distributions, although there are examples of asymmetric ones (see for example Refs. [22,41]). However, as can be seen in Fig. 3, the Gamow-

state spectra are always slightly asymmetric. Such asymmetry is not part of any background, but arises from the energy dependence of the matrix element. Nevertheless, for sharp resonances the asymmetry is small.

Experimental decay energy spectra are often fitted with a Breit-Wigner distribution that has an energy-dependent width, as was done in Refs. [14,22,25,28,30]. It seems therefore pertinent to discuss the similarities and differences between Eq. (3) and the Breit-Wigner distribution with energy-dependent width. First, both approaches yield quasi-Lorentzian peaks. However, in the case of Eq. (3), the Lorentzian is distorted by the matrix element of the interaction, whereas in the case of the Breit-Wigner distribution with energy-dependent width the distortion is produced by the energy dependence of the width. Second, a fit of the experimental decay energy spectrum (after deconvolution of the experimental error) using Eq. (3) would yield quantitatively different resonant energies and widths than using the Breit-Wigner distribution with energy-dependent width. Third, and most importantly, an energy-dependent width $\Gamma(E)$ implies an energy-dependent lifetime $\tau(E) = \frac{\hbar}{\Gamma(E)}$. Thus, although from a data-analysis point of view the Breit-Wigner distributions with energy-dependent width may not seem very different from Eq. (3), from a theoretical point of view they imply that resonances have different lifetimes for different energies. By contrast, when one describes a resonance by a Gamow state and its decay energy spectrum by Eq. (3), the (mean) lifetime is given by $\tau_R = \frac{\hbar}{\Gamma_R}$, and it is an intrinsic property of the resonance that doesn't depend on its energy. Four, instead of the pole width Γ_R being energy dependent, in the Gamow-state approach what depends on the energy is the differential decay width $d\bar{\Gamma}(E)/dE$ of Eq. (1), and such dependence takes into account that the resonance couples to the continuum with different strengths at different energies, while at the same time Γ_R , and therefore τ_R , are energy independent.

In principle, it is possible to test experimentally whether Eq. (3) or the Breit-Wigner distribution with energy-dependent width should be used as the true theoretical decay energy distribution of resonances. One could prepare the resonance at different energies, measure the mean lifetime for each energy, and check whether the lifetime changes with energy (as in Breit-Wigner distributions with energy-dependent width) or not (as in Eq. (3)).

5 Conclusions

Decay energy spectra of radioactive nuclei are routinely measured, and theoretical nuclear models should be able to predict such spectra. Within the limitations of a simple two-body model of ^{25}O , we have shown that the Gamow-state description of resonances is able to produce such spectra. We have modeled the ^{25}O nucleus as a valence neutron interacting with an ^{24}O core, and applied

the formalism of Ref. [18] to obtain the decay spectra of the ground and first-excited states. The resulting spectra have a quasi-Lorentzian peak centered around the resonant energy, and are qualitatively similar to those of simpler models [19], another example of the universality of resonance phenomena. We have also seen that the fits of experimental decay energy spectra that use a Breit-Wigner distribution with energy-dependent width are different, both quantitatively and phenomenologically, from fits that use the Gamow-state approach. In particular, the Breit-Wigner distributions with energy-dependent width imply an energy-dependent lifetime, whereas in the Gamow-state approach the lifetime is energy independent. We can, in principle, use the energy (non)dependence of the lifetime τ_R of a resonance to check whether the Gamow-state decay spectrum or the Breit-Wigner distribution with an energy-dependent width should be used as the true theoretical decay energy spectrum.

There are several ways in which the results of the present paper can be expanded. The most obvious one is the calculation of the decay energy spectrum of an unstable nucleus using the Gamow Shell Model. In particular, for ^{25}O , most of the ingredients needed to calculate the decay energy spectrum have already been obtained [21, 28], and it should be possible to obtain theoretical decay energy spectra that can be compared with experimental ones after deconvoluting the experimental error. Another way to extend the results of the present paper is by applying the Gamow-state description of decay energy spectra to multi-channel problems. There are methods to calculate the partial decay widths and branching fractions in a multi-channel system [42], but the calculation of the decay energy spectrum of a multi-channel potential is still awaiting.

Acknowledgements

The work of R.I.B. was supported by the National Council of Research PIP-625 (CONICET, Argentina).

A Appendix A: An almost delta-shell potential

In this Appendix, we will explain in what sense the potential $V_a(r)$ of Eq. (11) can be considered the delta-shell potential of strength $-V_0$ when a tends to zero.

Let us consider the set of functions $K_n(r)$ defined as

$$K_n(r) = -\frac{df_n(r)}{dr} = -\frac{d}{dr} \left(\frac{1}{1 + e^{n(r-R)}} \right) = n \frac{e^{n(r-R)}}{(1 + e^{n(r-R)})^2}, \quad (\text{A.1})$$

where n corresponds to $1/a$ in Eq. (11). Intuitively, $-f_n(r)$ tends to a unit-step function located at $r = R$ when n tends to infinity (i.e., when a tends to zero), so its derivative $K_n(r)$ should tend to the Dirac delta function $\delta(r - R)$.

In order for $K_n(r)$ to tend to the Dirac delta function, two conditions are usually required:

- (i) When n tends to infinity, the functions $K_n(r)$ tend to zero everywhere, except at $r = R$, where they diverge.
- (ii) The functions $K_n(r)$ are normalized to 1.

Condition (i) is clearly satisfied. In order to check condition (ii), let us calculate the following integral:

$$\int_{r_{\min}}^{\infty} K_n(r) dr = -[f_n(r)]_{r_{\min}}^{\infty} = \frac{1}{1 + e^{n(r_{\min}-R)}}. \quad (\text{A.2})$$

If $r_{\min} = -\infty$, then $\int_{-\infty}^{\infty} K_n(r) dr = 1$, condition (ii) is satisfied, and $K_n(r)$ tends to $\delta(r - R)$ when n tends to infinity. However, in our case $r_{\min} = 0$, $\int_0^{\infty} K_n(r) dr = \frac{1}{1 + e^{-nR}} \neq 1$, and therefore the functions $K_n(r)$ do not satisfy condition (ii). Nevertheless, as n becomes large, e^{-nR} is very small, and $\int_0^{\infty} K_n(r) dr = \frac{1}{1 + e^{-nR}}$, although not equal to 1, is very close to 1, and we have that for the purposes of the present paper the functions $K_n(r)$ become the delta function as n tends to infinity. This is why the potential $V_a(r)$ of Eq. (11) can be considered an almost delta-shell potential of strength $-V_0$.

We can formalize the above discussion even further by using the theory of distributions [43].

Definition. A set of functions $K_n(x)$ is a singular kernel that approximates the delta function at the origin if

$$\lim_{n \rightarrow \infty} \int_{-\infty}^{\infty} K_n(x) \varphi(x) dx = \varphi(0) \quad (\text{A.3})$$

for any test function φ .

In bra-ket notation Eq. (A.3) can be written as

$$\lim_{n \rightarrow \infty} \langle K_n | \varphi \rangle = \langle \delta | \varphi \rangle = \varphi(0). \quad (\text{A.4})$$

Thus, definition (A.3) is the mathematical formalization of calculating the Dirac delta function as the limit of functions.

Theorem. *Let $K_n(x)$ be a sequence of locally integrable functions that satisfy the following conditions:*

- (1) *There exists a positive s such that $K_n(x) \geq 0$ when $|x| < s$.*
- (2) *K_n converges uniformly to zero in any set $0 < x_0 \leq |x| \leq 1/x_0$ for any $x_0 > 0$.*
- (3) *$\lim_{n \rightarrow \infty} \int_{|x| \leq x_0} K_n(x) dx = 1$ for any $x_0 > 0$.*

Then the sequence $K_n(x)$ is a singular kernel that tends to the delta function at the origin as $n \rightarrow \infty$.

Condition (2) means that as n tends to infinity, the tails of $K_n(x)$ become vanishingly small. Condition (3) means that as n tends to infinity, $K_n(x)$ is concentrated at the origin.

To apply the theorem to the functions in Eq. (A.1), we need to use $x = r - R$ and $x_0 = r_0 - R > 0$. We will first apply the theorem to the case that r runs over the whole real line. Condition (1) is clearly satisfied. When $x = r - R$ is negative, condition (2) is also clearly satisfied. When $x = r - R$ is positive, we have that

$$K_n(x) = n \frac{e^{n(r-R)}}{(1 + e^{n(r-R)})^2} < n \frac{1}{e^{n(r-R)}} < n \frac{1}{e^{n(r_0-R)}} \xrightarrow[n \rightarrow \infty]{\text{uniformly}} 0. \quad (\text{A.5})$$

Hence, condition (2) is also satisfied when $x > 0$. Condition (3) is satisfied as well:

$$\int_{-x_0}^{x_0} K_n(x) dx = -[f_n(x)]_{-x_0}^{x_0} = \frac{-1}{1 + e^{n(r_0-R)}} + \frac{1}{1 + e^{-n(r_0-R)}} \xrightarrow[n \rightarrow \infty]{} 1 \quad (\text{A.6})$$

However, in our case r is positive, x is greater than $-R$, and therefore the above theorem does not apply as stated. Nevertheless, when n becomes large, the tails of $K_n(r)$ are so small when $r < 0$ that conditions (2) and (3) are satisfied for our purposes, and we have that the sequence $K_n(r)$ tends to $\delta(r - R)$ when n tends to infinity.

References

- [1] I. Tanihata, H. Hamagaki, O. Hashimoto, Y. Shida, N. Yoshikawa, Phys. Rev. Lett. **55** (1986) 2676.

- [2] B. Jonson, Phys. Rep. **389** (2003) 1.
- [3] T. Baumann, A. Spyrou, M. Thoennessen, Rep. Prog. Phys. **75** (2012) 036301.
- [4] I. Tanihata, H. Savajols, R. Kanungo, Prog. Part. Nucl. Phys. **68** (2013) 215.
- [5] J. Okolowicz, M. Ploszajczak, I. Rotter, Phys. Rep. **374** (2003) 271.
- [6] A. Volya, V. Zelevinsky, Phys. Atomic Nuclei **77** (2014) 969.
- [7] N. Michel, W. Nazarewicz, M. Ploszajczak, T. Vertse, J. Phys. G: Nucl. Part. Phys. **36** (2009) 013101.
- [8] S.J. Freedman, et al., Nuclear Physics. Exploring the Heart of Matter, National Research Council of the National Academies, The National Academy Press. Washington, D.C. (2013).
- [9] A.C. Mueller, An overview of radioactive beam facilities, Proceedings of EPAC, Vienna, Austria (2000).
- [10] R. Bennett, et al., Radioactive Nuclear Beam Facilities, The NuPECC Working Group on Radioactive Nuclear Beam Facilities, NuPECC Report (2000).
- [11] Y. Blumenfeld, T. Nilsson, P. Van Duppen, Phys. Scripta **T152** (2103) 014023.
- [12] T. Motobayashi, EPJ Web of Conferences **66** (2014) 01013.
- [13] D. Perez-Loureiro, et al., Phys. Rev. C **93** (2016) 064320.
- [14] M. Vandebrouck, et al. (R3B Collaboration), Phys. Rev. C **96** (2017) 054305.
- [15] A. Spyrou, et al., Phys. Lett. B **683** (2010) 129.
- [16] A. Spyrou, et al., Phys. Rev. Lett. **108** (2012) 102501.
- [17] M. Thoennessen, et al., Act. Phys. Pol. B **44** (2013) 543.
- [18] R. de la Madrid, Nucl. Phys. A **940** (2015) 297.
- [19] R. de la Madrid, Nucl. Phys. A **962** (2017) 24.
- [20] R. Dungan, et al., Phys. Rev. C **93** (2016) 021302(R).
- [21] K. Fossez, J. Rotureau, N. Michel, W. Nazarewicz, Phys. Rev. C **96** (2017) 024308.
- [22] C.R. Hoffman, et al., Phys. Lett. B **672** (2009) 17.
- [23] M.D. Jones, et al., Phys. Rev. C **92** (2015) 051306(R).
- [24] W.F. Rogers, et al., Phys. Rev. C **92** (2015) 034316.
- [25] C.R. Hoffman, et al., Phys. Rev. Lett. **100** (2008) 152502.
- [26] C. Caesar, Phys. Rev. C **88** (2013) 034313.
- [27] Y. Kondo, et al., Phys. Rev. Lett. **116** (2016) 102503.

- [28] M.D. Jones, et al.;
`{\sf\protect\vrulewidth0pt\protect\href{http://arxiv.org/abs/1710.04706}{arXiv:1710.04706}}`
- [29] E. Lunderberg, Phys. Rev. Lett. **108** (2012) 142503.
- [30] Z. Kohley, et al., Phys. Rev. C **87** (2013) 011304(R).
- [31] G. Gamow, Z. Phys. **51** (1928) 204.
- [32] J.R. Taylor, Scattering Theory, John Wiley & Sons (1972).
- [33] T. Vertse, K.F. Pal, Z. Balogh, Comput. Phys. Commun. **27** (1982) 309.
- [34] L.Gr. Ixaru, M. Rizea, T. Vertse, Comput. Phys. Commun. **85** (1995) 217.
- [35] R.J. Liotta, E. Maglione, N. Sandulescu, T. Vertse, Phys. Lett. B **367** (1996) 1.
- [36] <https://www.wolfram.com/mathematica/>
- [37] Numerical Recipes, <http://apps.nrbook.com/fortran/index.html>.
- [38] A. Volya, V. Zelevinsky, Phys. Rev. C **74** (2006) 064314.
- [39] Evaluated nuclear structure data file, <http://www.nndc.bnl.gov>.
- [40] H. Frauenfelder, E.M. Henley, Subatomic Physics, Prentice Hall (1991).
- [41] The LHCb Collaboration, arXiv:1711.05490.
- [42] S. Rakityansky, J. Phys.: Conf. Ser. **915** (2017) 012008.
- [43] L. Schwartz, Mathematics for the Physical Sciences, Hermann (1966).